

# A stable artificial protective layer for high capacity dendrite-free lithium metal anode

Zhipeng Wen<sup>1,§</sup>, Yueying Peng<sup>1,§</sup>, Jianlong Cong<sup>1</sup>, Haiming Hua<sup>1</sup>, Yingxin Lin<sup>2</sup>, Jian Xiong<sup>1</sup>, Jing Zeng<sup>1</sup>, and Jinbao Zhao<sup>1,2</sup> (✉)

<sup>1</sup> State Key Lab of Physical Chemistry of Solid Surfaces, Collaborative Innovation Centre of Chemistry for Energy Materials, State-Province Joint Engineering Laboratory of Power Source Technology for New Energy Vehicle, Engineering Research Center of Electrochemical Technology, Ministry of Education, College of Chemistry and Chemical Engineering, Xiamen University, Xiamen 361005, China

<sup>2</sup> College of Energy & School of Energy Research, Xiamen University, Xiamen 361102, China

<sup>§</sup> Zhipeng Wen and Yueying Peng contributed equally to this work.

© Tsinghua University Press and Springer-Verlag GmbH Germany, part of Springer Nature 2019

Received: 12 May 2018 / Revised: 24 June 2019 / Accepted: 13 July 2019

## ABSTRACT

The metallic lithium (Li) is considered as the most promising anode material for high-energy batteries. Nevertheless, the uncontrollable growth of Li dendrite and unstable electrolyte/electrode interface still hinder the development of Li-based battery. In this work, a novel strategy has been proposed to stabilize Li anode by *in-situ* polymerizing polypyrrole (PPy) layer on Ni foam (PPy@Ni foam) as an artificial protective layer. The PPy protective layer can effectively decrease the contact between Li metal and electrolyte during cycling. In addition, the morphology characterization shows that the PPy layer can help the even Li deposition underneath the layer, leading to a dendrite-free Li anode. As a result, when deposited 2 mAh·cm<sup>-2</sup> Li metal, the PPy@Ni foam can keep stable Coulombic efficiency (99%) during nearly 250 cycles, much better than the pure Ni foam (100 cycles). Even in the case of the Li capacity of 10 mAh·cm<sup>-2</sup>, the stable cycling performance for 60 cycles can still be achieved. Furthermore, when assembled with LiFePO<sub>4</sub> material as the cathode for a full cell, the PPy@Ni foam can keep high capacity retention of 85.5% at 500 cycles. In our work, we provide a simple and effective method to enhance the electrochemical performances of Li metal-based batteries, and reveal a new avenue to design three-dimensional (3D) metallic current collector for protecting the Li metal anode.

## KEYWORDS

high capacity, polypyrrole layer, Li metal, artificial protective layer, dendrite-free anode

## 1 Introduction

Driven by the increasing demand for high-energy batteries, much attention has been paid to the lithium (Li) metal anode [1, 2]. Metallic Li is considered as an ideal anode material due to its advantages such as extremely high specific capacity (3,860 mAh·g<sup>-1</sup>), low reduction potential (−3.04 V vs. the standard hydrogen electrode) and low density [3, 4]. Despite these considerable advantages, the commercial applications of Li anode-based batteries are still hindered by following intrinsic problems: (1) The unstable solid electrolyte interface (SEI) of Li anode causes repeated exposure of fresh Li surface, resulting in the excessive consumption of electrolyte; (2) the large volume expansion of Li during charging/discharging in turn triggers the stability of SEI more seriously, and causes the uneven Li stripping and plating; (3) the uncontrollable growth of Li dendrite may break off from the Li root and form “dead Li”, resulting in the loss of Li metal and increase in cell impedance. To make matters worse, the Li dendrite may impale the separator, resulting in serious safety issues. As a result, the Li anode suffers from low Coulombic efficiency, poor cycling stability and safety hazards [5, 6].

To address these challenges, plenty of efforts have been taken to inhibit the uncontrollable growth of Li dendrite by the modifications of SEI film on Li anode [7–11]. The Li metal can spontaneously form a SEI film with organic electrolyte due to its high reactivity [12–14]. Though the SEI film can play as a protective layer to prevent

the further reaction, it cannot adapt the large volume expansion during cycling, leading to the collapse of SEI film and the growth of Li dendrite eventually [15]. An ideal SEI film should possess not only suitable flexibility to relieve the volume expansion, but also certainly mechanical strength to resist the penetration of Li dendrite [16, 17]. To obtain such ideal SEI, much work has been carried out mainly based on two aspects: electrolyte project and interface modification. On the one hand, some suitable electrolyte systems have been selected to *in-situ* form stable SEI on the Li surface, including adding electrolyte additives, changing Li salts and solvents [18–23]. For example, the electrolyte additive can participate in the SEI formation by *in-situ* reacting with Li anode to generate functional compounds, such as high modulus interfacial polymers, alloy and inorganic salts [24–31]. Thus, a trace amount of electrolyte additive can greatly help Li anode construct an effective SEI. However, as it is difficult to completely prevent the reaction of Li and electrolyte, there is still continuous consumption of electrolyte and additive, which makes it challenge to obtain long cycling stability [32]. On the other hand, the interface modification has been adopted by directly forming artificial SEI film on the Li metal via chemical reaction or physical methods [33–37]. As the artificial SEI is produced by pre-treatment of Li anode or synthesized individually, the structure and components of artificial SEI film can be controlled effectively [38]. However, as the artificial SEI is normally constructed on the Li anode surface, both strict experimental conditions and equipment

are required. Therefore, it is necessary to find a simple and valid strategy to protect Li metal.

Here, we developed a novel method to protect Li anode by *in-situ* constructing a polypyrrole (PPy) protective layer on the Ni foam current collector (PPy@Ni foam) under which the Li deposits. The PPy is chosen as a polymer protective layer and the Ni foam is used as current collector due to its light weight and large specific surface area [39]. These results show that the *in-situ* polymerized PPy not only shows chemical stability during long-term cycling, but also has strong protection in Li metal. As a result, the PPy@Ni foam exhibits outstanding electrochemical performance. When deposited  $2 \text{ mAh}\cdot\text{cm}^{-2}$  at current density of  $1 \text{ mA}\cdot\text{cm}^{-2}$ , a high Coulombic efficiency of 99% can be still maintained after 250 cycles. Using the limited Li/LiFePO<sub>4</sub> (LFP) as the anode/cathode material to assemble a full cell, a stable cycling ability can be obtained, with capacity retention of 85.5% after 500 cycles. The strategy of constructing a preformed layer on the current collector plays a vital role on protecting Li anode, opening a new platform for designing a stable Li anode.

## 2 Experimental

### 2.1 Preparation of the PPy@Ni foam

The commercial Ni foam (1.5 mm in thickness, 0.2 mm in pore diameter) was washed first by ultrasonically in acetone to remove the impurity. Then 0.136 g (NH<sub>4</sub>)<sub>2</sub>S<sub>2</sub>O<sub>8</sub> (XILONG SCIENTIFIC, > 98%) was dissolved in 40 mL deionized water and alcohol mixed solution (1/1, in volume), and the solution was stirred for 10 min to be well mixed. After that, 54  $\mu\text{L}$  pyrrole (Aladdin, > 99.7%) was added to the obtained solution. Before immersed in the solution for 8 h, the Ni foam was cut into a square with a side length of 8 cm, followed by washing with water and alcohol mixed solution (1/1, in volume) several times until the washed solution was clear. After drying, the PPy@Ni foam was cut into small disks (12 mm in diameter) as current collector for later use.

### 2.2 Characterization methods

The scanning electron microscopy (SEM) images were characterized by HITACHI S-4800 at 10 kV. The Fourier transform infrared (FTIR) spectra were collected using a Nicolet IS5 spectrometer (Thermo Fisher). The X-ray photoelectron spectra (XPS) data were obtained by the X-ray photoelectron spectroscopy (PHI QUANTUM 2000).

### 2.3 Electrochemical measurements

The CR2032 cell was used to test Coulombic efficiency and full-cell properties, assembled in argon filled glovebox. The commercial 301 carbonate electrolyte was purchased from Zhangjiagang Guotai-Huarong New Chemical Materials Co., Ltd. The solution of 1.0 M bis(trifluoromethanesulfony)mide lithium (LiTFSI) dissolved in 1,3-dioxolane (DOL) and dimethyl ether (DME) (DOL:DME = 1:1, in volume) with 2 wt.% LiNO<sub>3</sub> as the additive to promote the formation of stable SEI film was used as the electrolyte, the pristine Ni foam or PPy@Ni foam current collector and bare Li metal (12 mm in diameter) were used as the working electrode and counter electrode, respectively.

To test Li stripping/plating Coulombic efficiency, 80  $\mu\text{L}$  ether electrolyte was consumed to assemble half-cell. The cell was followed by electrodepositing different amounts of Li (1, 2, 5, and 10  $\text{mAh}\cdot\text{cm}^{-2}$ ) at the current density of  $1 \text{ mA}\cdot\text{cm}^{-2}$  onto the pristine Ni foam or PPy@Ni foam and stripping Li until the voltage reaches 0.5 V (vs. Li<sup>+</sup>/Li) at same current density.

To test the cycling performance of symmetric cell with pure Ni foam and PPy@Ni foam. The pure Ni foam and PPy@Ni foam were predeposited  $2 \text{ mAh}\cdot\text{cm}^{-2}$  Li metal with  $1 \text{ mA}\cdot\text{cm}^{-2}$  current density to be used. And then the Li-Ni was washed by DME solution and

paired with another predeposited Ni foam current to assemble cell. The symmetric cell was cycled with current density of  $1 \text{ mA}\cdot\text{cm}^{-2}$  and deposition capacity of  $1 \text{ mAh}\cdot\text{cm}^{-2}$ .

To test full-cell properties, the LFP and Li metal were used as the cathode and the anode, respectively. The LFP, acetylene black, poly(vinyl difluoride) were mixed in N-methyl pyrrolidone (NMP) by the weight of 8:1:1, and stirred overnight. Then the slurry was spread on the aluminum foil evenly. After drying, the product was cut into small round disk (12 mm in diameter). The pristine Ni foam or PPy@Ni foam could be electrodeposited Li metal ( $3 \text{ mAh}\cdot\text{cm}^{-2}$ ) before used as the anode. Then the Ni foam deposited Li metal and LFP electrode were assembled full-cell for test electrochemical properties.

### 2.4 Computational details

All the quantum chemistry calculations were performed using Gaussian09 E01 software [40]. The geometries of all the molecules were optimized in gas using M06-2X-D3[41, 42] density functional with def2-SVP [43] basis set. Single point energy of all optimized geometries was further calculated with def2-TZVP basis set [43]. Vibration analysis was performed to identify all the geometries as minimum (0 imaginary frequency) or transition (1 imaginary frequency) and gain the thermal corrections to Gibbs free energy at 298.15 K and 1 atm. A continuum solvation model SMD [44] with its parameterized level M05-2X/6-31G\* [45–48] was used to calculate Gibbs free energy of dissolution. The relative dielectric constant ( $\epsilon$ ) of the electrolyte was 7.2 and parameters of non-polar parts were same as diethyl ether. All the energy discussed in this paper is the free energy in solution. An NVT semi-empirical molecular dynamics simulation based on GFN2-xtb [49] at 298.15 K for 100 ps was performed using xtb software. The visualization of all the geometries was performed using VMD [50] software. A chain containing six pyrrole monomer units was used to represent polypyrrole and the active free energy of migration was calculated from Li<sup>+</sup> migrating on the middle two rings.

## 3 Results and discussion

### 3.1 Morphology and characterization of the PPy@Ni foam

The schematic illustration of different Li deposition process on Ni foam is illustrated in Fig. 1(a). For the pristine sample, the Li deposition on skeleton is unregulated, resulting in the growth of Li dendrite. In addition, the Li root prefers to dissolve early, and separates from the Li metal anode. The isolated Li dendrite is called “dead Li” which causes the increase in cell polarization. Moreover, the high surface area of Ni foam needs more electrolytes to construct SEI film, causing the limited cycling lifespan. By contrast, the Li deposition is more uniform, and the higher utilization percentage of lithium metal surface can be achieved after coating with PPy artificial protective layer. Therefore, it contributes to the homogeneous distribution of the Li<sup>+</sup>, and significantly increases the utilization of Li metal surface. The decrease in local current density benefits from higher utilization percentage, which leads to the suppression in Li dendrite. Moreover, the PPy protective layer can lower the parasitic reactions between Li metal with electrolyte. In addition, it can physically separate the high reactive Li anode and electrolyte, resulting in the improvement of cycling performance/Coulombic efficiency.

To comprehend the morphologies of Ni foam sample, the optical photographs and SEM images have been collected. Figure 1(b) shows the optical photograph of pristine Ni foam. The results show that the pristine Ni foam exhibits metallic white appearance, while the color changes to black after coating PPy protective layer (Fig. 1(e)). The SEM is conducted to further observe their morphologies. From Figs. 1(c) and 1(d), the low-magnification SEM image shows that the pristine Ni foam has three-dimensional (3D) porous structure



**Figure 1** (a) The schematic illustration of different Li deposition process. Optical photographs of (b) pristine Ni foam and (e) PPy@Ni foam. SEM images of (c) and (d) pristine Ni foam and (f) and (g) PPy@Ni foam.

and the high-magnification SEM image indicates the smooth surface of Ni foam. Additionally, the black dots occur on the surface of pure Ni foam don't affect the properties (Fig. S1 in the Electronic Supplementary Material (ESM)). By contrast, the PPy@Ni foam exhibits a rough morphology with a folded layer (Figs. 1(f) and 1(g)), indicating the successful coating of PPy layer. In addition, it can be still found that the 3D porous structure of the PPy@Ni foam is well maintained, ensuring the fast pathway for ions and electrons to transport. To investigate the uniformity of PPy protective layer on Ni foam, the corresponding element mapping of PPy@Ni foam was carried out (Fig. S2 in the ESM). The homogeneous distribution of carbon element and nickel element can clearly prove the uniformity of PPy protective layer. The FTIR spectra have been used to further demonstrate the existence of PPy on the Ni foam, and the result confirms the 2D structure of PPy protective layer on the Ni foam (Fig. S3 in ESM).

The SEM images and element mapping of PPy@Ni foam before and after the deposition of Li metal have been accomplished to investigate the structure stability of PPy@Ni foam. As Fig. 2(a) shows, the PPy protective layer is quite thin so that does not influence the advantage of 3D porous structure. As shown in the high magnification SEM image of PPy@Ni foam (Fig. S4 in the ESM), the thickness of PPy protection layer is about 370 nm. What's more, the light weight of PPy layer (0.83 mg) can contribute to high energy Li metal-based battery (Table S1 in the ESM). In addition, the PPy layer has a strong chemical stability, which ensures the structure stability of PPy@Ni foam (Fig. 2(d)). From the element mapping of PPy@Ni foam after the deposition of Li, there are obvious voids between the PPy protective layer and Li metal, as shown by the red line in Fig. 2(e). This indicates that  $\text{Li}^+$  passes through the PPy protective layer and deposits on the Ni foam due to low conductivity of PPy protective layer. The advantages of PPy protective layer improve the cycling stability of Li metal-based batteries. To explore the properties of PPy protective layer, the XPS measurements have been carried out to study the surface composition of Ni foam. As illustrated in Fig. 2(c), the main N peak at 400.1 eV can correspond to the pyrrole-N functional group, indicating the major existence of PPy on PPy@Ni foam. Except that, the pyridine-N peak at 398.1 eV may originate from the side products of polymerization [29]. As shown in the previous studies, the organic electrolyte and Li salts influence the organic composition and inorganic composition of surface on Li metal, separately [40, 51, 52]. After the influence of LiTFSI-based electrolyte, the component of surface on the Li metal is mainly composed of LiF and  $\text{RCO}_2\text{Li}$ , as illustrated in Fig. 2(f) [30, 31]. By comparison, the surface of Li metal with the PPy@Ni foam mainly consists of LiF and  $\text{Li}_3\text{N}$ , as illustrate in Li 1s spectra. Compared with the pure Ni foam (55.7 eV) [53, 54], the Li-F of PPy@Ni foam exhibits lower binding energy (55.5 eV), indicating electron transfer from the fluorine atoms to the electropositive lithium, resulting from the formation of Li-N bond [55, 56]. The difference in component indicates that the PPy layer can effectively prevent the Li metal from contacting with electrolyte. Therefore, the PPy protective layer plays an important role in Li metal anode protection.

### 3.2 Electrochemical performances of the Li/PPy@Ni cell

To evaluate cycling stability performance, the pristine Ni foam or PPy@Ni foam current collector has been assembled with the Li foil. During the measurements, the current density has been cycled at  $1 \text{ mA}\cdot\text{cm}^{-2}$  for both pristine Ni foam and PPy@Ni foam. With Li

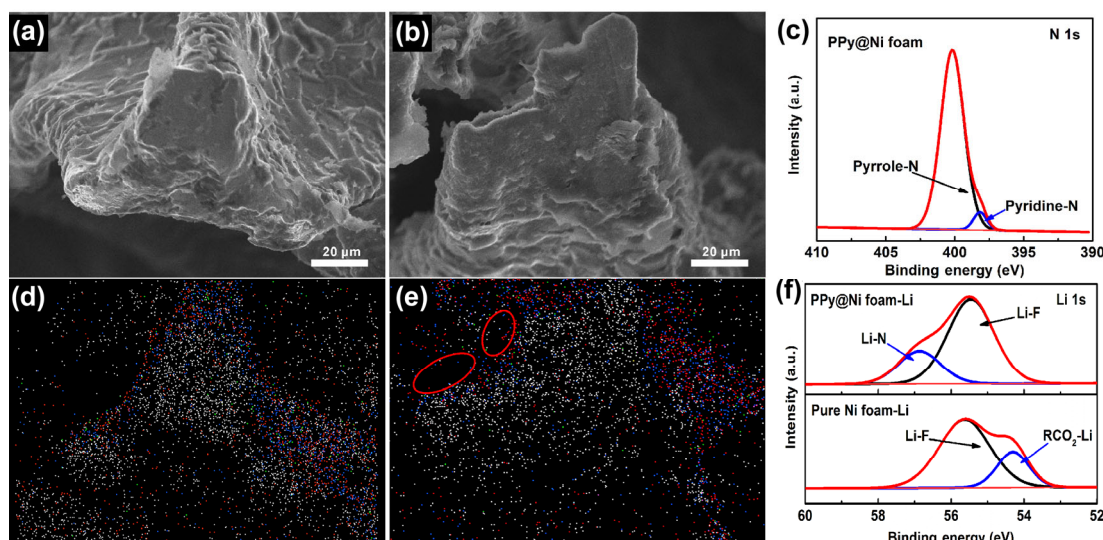


**Figure 2** (a) and (d) The SEM image and the corresponding element mapping of PPy@Ni foam. (b) and (e) The SEM image and the corresponding element mapping of PPy@Ni foam after depositing Li metal. White plot (Ni), blue plot (C), orange plot (O) and green plot (N). (c) The N 1s XPS of the surface of PPy@Ni foam. (f) The Li 1s XPS of the SEI layer of current collector after depositing Li metal.

deposition of  $2 \text{ mAh}\cdot\text{cm}^{-2}$ , the pristine Ni foam exhibits a high initial Coulombic efficiency (92.27%), which is obviously higher than that of PPy@Ni foam (81.95%). However, the Coulombic efficiency of pristine Ni foam exhibits a rapidly decrease after 100 cycles and fails after 150 cycles. By contrast, the PPy@Ni foam increases to 97% after 10 cycles, and shows a stable Coulombic efficiency of 99% for nearly 250 cycles. The poor cycling stability performance of pristine Ni foam is mainly due to the unstable SEI film which leads to the loss of Li metal active material during cycling. Nevertheless, the stable Coulombic efficiency of PPy@Ni foam has proved the protection of PPy protective layer in Li metal. Meanwhile, the PPy@Ni foam can also keep stable cycling performance in the case of carbonate electrolyte (Fig. S5 in the ESM). On the other hand, the Li deposition amounts in previous reports are mainly 0.5 or  $1.0 \text{ mAh}\cdot\text{cm}^{-2}$ , which are relatively low and cannot meet the demands for commercialization (Table S2 in the ESM). Therefore, the higher Li deposition capacities with 5 and  $10 \text{ mAh}\cdot\text{cm}^{-2}$  Li deposition have been measured in our work (Figs. 3(b) and 3(c)). The results show that the pristine Ni foam fails rapidly after 30 cycle with  $5 \text{ mAh}\cdot\text{cm}^{-2}$  Li deposition and 11 cycles with  $10 \text{ mAh}\cdot\text{cm}^{-2}$  Li deposition (Figs. S6 and S7 in the ESM). By contrast, the Coulombic efficiency of PPy@Ni foam can stabilize at 98% after 90 cycles with  $5 \text{ mAh}\cdot\text{cm}^{-2}$  Li deposition. When deposited  $10 \text{ mAh}\cdot\text{cm}^{-2}$  Li metal, the lifespan of Ni foam can be improved

over six times by using PPy protective layer. The higher Coulombic efficiency of PPy@Ni foam than the pristine Ni foam has proved that the PPy protective layer can stabilize the electrolyte/electrode interface effectively and reduce the loss of Li. In addition, the outstanding performance of the PPy@Ni foam in cycling lifespan indicates the important role of PPy protective layer in the suppression of Li dendrite.

To investigate the structure stability of SEI during prolonged cycling, the cell with different sample has been cycled at the current density of  $1 \text{ mA}\cdot\text{cm}^{-2}$  with the Li deposition capacity of  $2 \text{ mAh}\cdot\text{cm}^{-2}$ . The voltage gap between charge/discharge plateaus can reflect the difficulty of Li stripping/plating process on the current collector. The voltage profiles of pristine Ni foam and PPy@Ni foam have a similar shape, while the voltage gap between charge/discharge plateaus of pristine Ni foam is larger (Figs. 3(d) and 3(e)). From the further observation (Fig. 3(h)), the polarization of PPy@Ni foam is larger than pure Ni foam at the initial cycle due to the existence of artificial PPy protective layer [57]. However, the pristine Ni foam has demonstrated continuously increase voltage gap during cycling. Furthermore, the voltage gap of pristine Ni foam after 150 cycles ( $\sim 0.044 \text{ V}$ ) is also obviously larger than that of PPy@Ni foam ( $\sim 0.03 \text{ V}$ ). By contrast, the PPy@Ni foam exhibits a stable and low voltage gap between charge/discharge plateaus. What's more, the Li

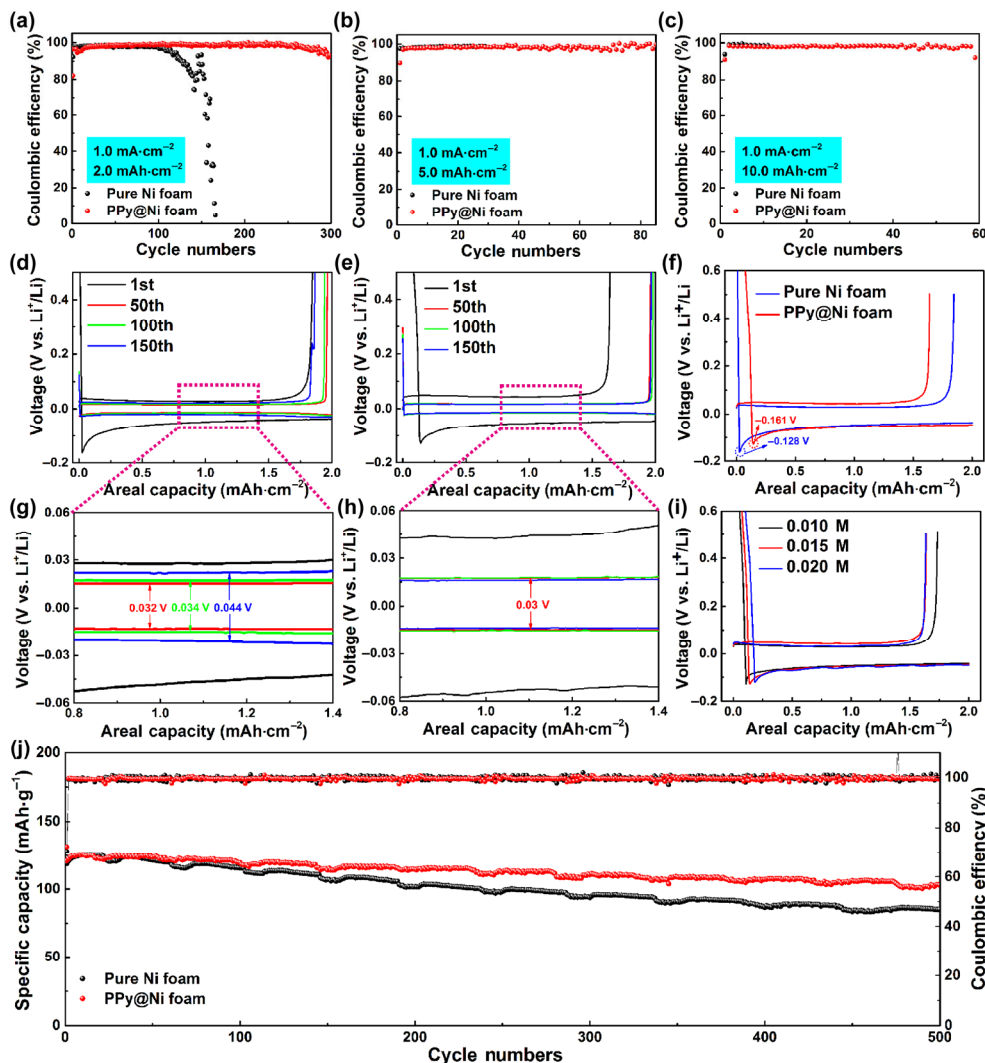


**Figure 3** Electrochemical performances of pristine Ni foam and PPy@Ni foam. The Coulombic efficiency of pristine Ni foam and PPy@Ni foam at the current density of  $1.0 \text{ mA}\cdot\text{cm}^{-2}$  with the Li deposition amount of (a) 2.0, (b) 5.0 and (c) 10.0  $\text{mAh}\cdot\text{cm}^{-2}$ . Voltage profiles of pristine Ni foam (d) and (g) and PPy@Ni foam (e) and (h) with the Li deposition amount of  $2.0 \text{ mAh}\cdot\text{cm}^{-2}$  in different cycles. (f) Voltage profiles of the first Li stripping/plating cycle on pristine Ni foam and PPy@Ni foam with the Li deposition amount of  $2.0 \text{ mAh}\cdot\text{cm}^{-2}$ . (i) Voltage profiles of PPy@Ni foam synthesized with different concentrations cycled with the Li deposition capacity of  $2 \text{ mAh}\cdot\text{cm}^{-2}$ . (j) The cycling performance of the full cell with pristine Ni foam and PPy@Ni foam.

deposition onto PPy@Ni foam has much lower nucleation overpotential ( $-0.128$  V) than that of pristine Ni foam current collector ( $-0.161$  V), which indicates the Li deposition become more easy with the PPy@Ni foam. Such small polarization in Li electrodeposit on the PPy@Ni foam can be attributed to the following reasons. On the one hand, the PPy protective layer can reduce the impedance originated by inhomogeneous distribution of  $\text{Li}^+$ , therefore, lead to the lower polarization. On the other hand, the PPy@Ni foam can inhibit the growth of Li dendrite effectively and avoid the continuous destruction of SEI film, resulting in the stable electrolyte/electrode interface and the changeless Li deposition overpotential. Last but not least, the PPy protective layer can help Li deposition and ensure fast  $\text{Li}^+$  transportation, contributing to the decrease of nucleation overpotential. To test the Li reaction kinetics, the cycling performances of symmetric Li metal cells with pristine Ni foam and PPy@Ni foam were carried out (Fig. S8 in the ESM) [58]. The symmetric cell was tested with the current density of  $1 \text{ mA}\cdot\text{cm}^{-2}$  and deposition capacity of  $1 \text{ mAh}\cdot\text{cm}^{-2}$ . The results indicated that the PPy@Ni foam exhibits lower Li plating/stripping overpotential, therefore owning faster reaction kinetic. Additionally, the electrochemical impedance spectroscopy (EIS) spectra are conducted with symmetric cells of pristine Ni foam and PPy@Ni foam (Fig. S9 in the ESM). As shown Fig. S9(a) in the ESM, the pure Ni foam and PPy@Ni foam exhibited nearly equal impedance, indicating cycled PPy protective layer doesn't affect the Li ion conductivity. While after 10 cycles, the PPy@Ni foam holds lower impedance, ensuring faster Li ion transportation (Fig. S9(b) in the ESM). As a result, the PPy protective layer can help faster reaction kinetic and stable cycling performance. Noticeable, the capacity hysteresis of Li nucleation reaction on the PPy@Ni foam is obviously higher at first cycle. To investigate the reason, the PPy@Ni foams synthesized with different concentrations have been characterized (Figs. S10–S16 in the ESM). As shown in Figs. S10 and S11 in the ESM, the thickness of PPy protective layer in  $0.010 \text{ M}$  PPy@Ni foam is evaluated about  $200 \text{ nm}$ , and the thickness of PPy protective layer in  $0.020 \text{ M}$  PPy@Ni foam is evaluated about  $520 \text{ nm}$ . The cycling performance of Li-Ni cell showed that the  $0.015 \text{ M}$  PPy@Ni foam exhibits excellent electrochemical cycling properties (Fig. S12 in the ESM). It can be obtained that PPy layer that is too thin or too thick cannot exert its protective effect on Li metal. The EIS spectra proved that the thickness of PPy protective layer had small impact on the electrochemical impedance (Fig. S16 in the ESM). At last, the different thickness of PPy@Ni foam was cycled at the current density of  $1 \text{ mA}\cdot\text{cm}^{-2}$  with the Li deposition capacity of  $2 \text{ mAh}\cdot\text{cm}^{-2}$ , as illustrated in Fig. 3(i). The capacity hysteresis of PPy@Ni foam increases from  $0.108$  to  $0.181 \text{ mAh}\cdot\text{cm}^{-2}$  when solution concentration increased. Therefore, it can be inferred that the PPy@Ni foam needs to complete the electrochemical lithiation at the initial cycle for constructing a chemically stable and ion conductive artificial protective layer. The detailed reason will be discussed in later section. In short, the improvement in cycling performance of Li anode-based battery with the PPy@Ni foam current collector can benefit from the suppression in Li dendrite.

Finally, the full cell has been assembled by using LFP as the cathode material to match with the pristine Ni foam and PPy@Ni foam current collector which all have predeposited  $3 \text{ mAh}\cdot\text{cm}^{-2}$  Li metal. To pair with limited Li anode, the mass loading of LFP in the test is  $2.56 \text{ mg}\cdot\text{cm}^{-2}$ . To further investigate the Li utilization of pristine Ni foam and PPy@Ni foam, the long term cycling performances of full cell was test with  $1.152 \text{ mA}\cdot\text{cm}^{-2}$  (Fig. 3(j)). The full cell with pristine Ni foam shows an initial capacity of  $118.8 \text{ mAh}\cdot\text{g}^{-1}$ , and decreases to  $84.7 \text{ mAh}\cdot\text{g}^{-1}$  after 500 cycles, meaning that the capacity retention is  $71.1\%$ . By contrast, the full cell with PPy@Ni foam exhibits better cycling performance with specific capacity of  $102.6 \text{ mAh}\cdot\text{g}^{-1}$  at 500 cycles, corresponding to the capacity retention of  $85.5\%$ . The better Li utilization for full cell with PPy@Ni foam proves that PPy protective layer can prevent the Li metal from contacting with

electrolyte, thus improving the Li utilization effectively.

### 3.3 Mechanism study

To explore the function of PPy protective layer in Li dendrite suppression, the SEM images have been recorded after cycled at current density of  $0.5 \text{ mA}\cdot\text{cm}^{-2}$  with different Li deposition capacities, as illustrated in Fig. 4. Compared with the initial morphology of pristine Ni foam (Fig. 2(c)), irregular Li deposition occurs on the surface of Ni foam when deposition capacity is  $1 \text{ mAh}\cdot\text{cm}^{-2}$  (Fig. 4(a)). As the Li metal continuously deposits onto the Ni foam, the Li dendrite appears due to the uneven Li deposition (Figs. 4(c) and 4(e)). The growth of Li dendrite can result in low Coulombic efficiency during cycling, and even cause the safety issues. In addition, the crack of SEI film begins to appear as a result of the inhomogeneous distribution of  $\text{Li}^+$ , which attitudes to the continuous consumption of Li metal and electrolyte during cycling. Besides, any parts of Ni foam are not covered with Li metal which aggravates the uneven Li deposition and leads to the unstable cycling performance [59]. In contrast, the PPy@Ni foam shows a flat and dendrite-free Li deposition, which attributes to the presence of PPy protective layer (Fig. 4(b)). Obviously, the folds of PPy@Ni foam start to disappear gradually, and the surface of PPy@Ni foam becomes more and more flat (Fig. 1(g)). It can be confirmed that the  $\text{Li}^+$  deposits below the PPy protective layer, and exhibits a flat and even Li deposition (Fig. 4(d)). Therefore, the PPy protective layer can function as an artificial protective layer to prevent Li metal contacting with electrolyte, resulting in the improvement of Coulombic efficiency. Simultaneously,

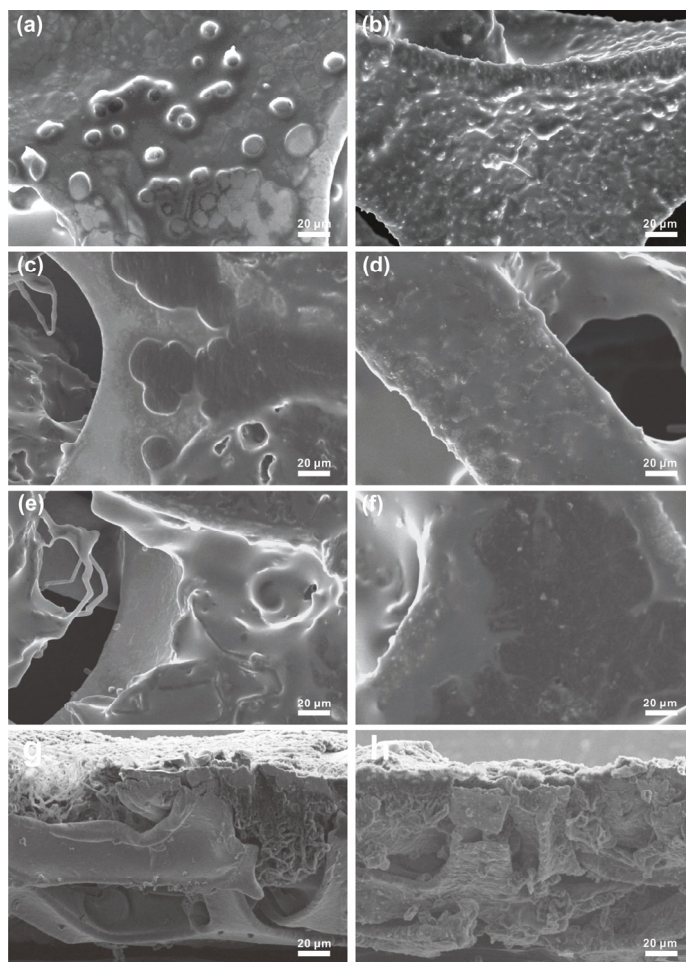


**Figure 4** The SEM images of different amounts of Li deposition on Ni foam sample. The SEM images of Li deposition with (a) 1, (c) 2, and (e)  $5 \text{ mAh}\cdot\text{cm}^{-2}$  on pristine Ni foam. The SEM images of Li deposition with (b) 1, (d) 2, and (f)  $5 \text{ mAh}\cdot\text{cm}^{-2}$  on PPy@Ni foam. The side view SEM images of (g) pristine Ni foam and (h) PPy@Ni foam when deposited  $10 \text{ mAh}\cdot\text{cm}^{-2}$  Li metal.

there are no any presences of Li dendrite, which prove the advantage of PPy protective layer in suppression Li dendrite (Fig. 4(f)). The previous study has showed that the majority of Li metal tends to accumulate and deposit on the bottom of Ni foam skeleton due to its high conductivity, leaving many parts of Ni foam not being used [60]. Therefore, the side view SEM images of pristine Ni foam and PPy@Ni foam when deposited  $10 \text{ mAh}\cdot\text{cm}^{-2}$  are illustrated in Fig. 4(g). Although with  $10 \text{ mAh}\cdot\text{cm}^{-2}$  Li metal, the bottom of Ni foam is still unoccupied. The inhomogeneous distribution of Li metal damages the advantages of 3D metallic current collector, leading to the unstable cycling performance with high capacity. By contrast, the Li metal can evenly distribute in the whole PPy@Ni foam current collector. It attributes to the homogeneous distribution of Li metal, which benefits from the isolation of PPy protective layer. In short, the PPy protective layer can help the even Li metal deposition and inhibit the growth of Li dendrite. Additionally, the PPy protective layer can increase the utilization of Ni foam current collector, and create a homogeneous distribution of Li metal. Therefore, it can contribute to the stable cycling performance of Li metal-based battery, especially at high Li metal capacity.

In order to investigate the stability of PPy protective layer on the Ni foam current collector during prolonged cycling, the morphologies of pristine Ni foam and PPy@Ni foam during cycling have been examined by the SEM as shown in Fig. 5. The pristine Ni foam and PPy@Ni foam current collector are cycled with the Li deposition capacity of  $5 \text{ mAh}\cdot\text{cm}^{-2}$ , as illustrated in Figs. 5(a) and 5(b). The SEM image of pristine Ni foam shows that the shape of SEI film is irregular and presents a dendritic trend. Therefore, the SEI film formed on the pristine Ni foam is uneven and unstable, and is easily damaged by the Li metal [61]. By comparison, the morphology of PPy@Ni foam has not changed after cycling, which confirms the structure stability of PPy protective layer. After undergoing 50 cycles, the morphology of Li metal on the pristine Ni foam is extremely heterogeneous with dendritic shapes (Figs. 5(c) and 5(e)). Such heterogeneous structure extremely influences the even Li metal deposition, and increases the risk of accident issues. By contrast, the flat surface and homogeneous distribution of Li metal are observed for the PPy@Ni foam (Fig. 5(d) and 5(f)). It can be obviously seen that the PPy protective layer still keep its initial shape. In short, the PPy protective layer can afford the volume change of Li metal after prolonged cycling and protect Li metal anode.

To understand the migration of  $\text{Li}^+$  on PPy protective layer, the quantum chemical calculations were carried out in Fig. 5(g). As the result shows,  $\text{Li}^+$  ions in the electrolyte are able to combine with the pyrrole ring by cation- $\pi$  interaction. The combining free energy is calculated to be  $-22.4 \text{ kJ}\cdot\text{mol}^{-1}$ , which indicates that the lithium salt in the solution is likely to be dispersed in the PPy. In addition, the PPy has continuous sites on the chain to combine  $\text{Li}^+$  ions, as it is a large conjugated system. The active free energy of  $\text{Li}^+$  ion migrating between the neighboring pyrrole rings is only  $18.1 \text{ kJ}\cdot\text{mol}^{-1}$ , which shows a fast reaction at room temperature. The migration reaction on a chain is also confirmed by a semi-empirical molecular dynamics simulation (Video ESM1). Combined with the experiment results, it is clear that the  $\text{Li}^+$  should finish a required process with PPy protective layer during charging, and then deposits beneath the PPy protective layer.

## 4 Conclusion

In this work, we find that the PPy layer can protect the Li metal anode effectively as an artificial protective layer. The results show that the high capacity lithium metal-based battery enables long cycle can be achieved. The PPy@Ni foam demonstrates an outstanding superiority in the cycling performance. With the Li deposition amount of  $2.0 \text{ mAh}\cdot\text{cm}^{-2}$ , the PPy@Ni foam can keep the stable average

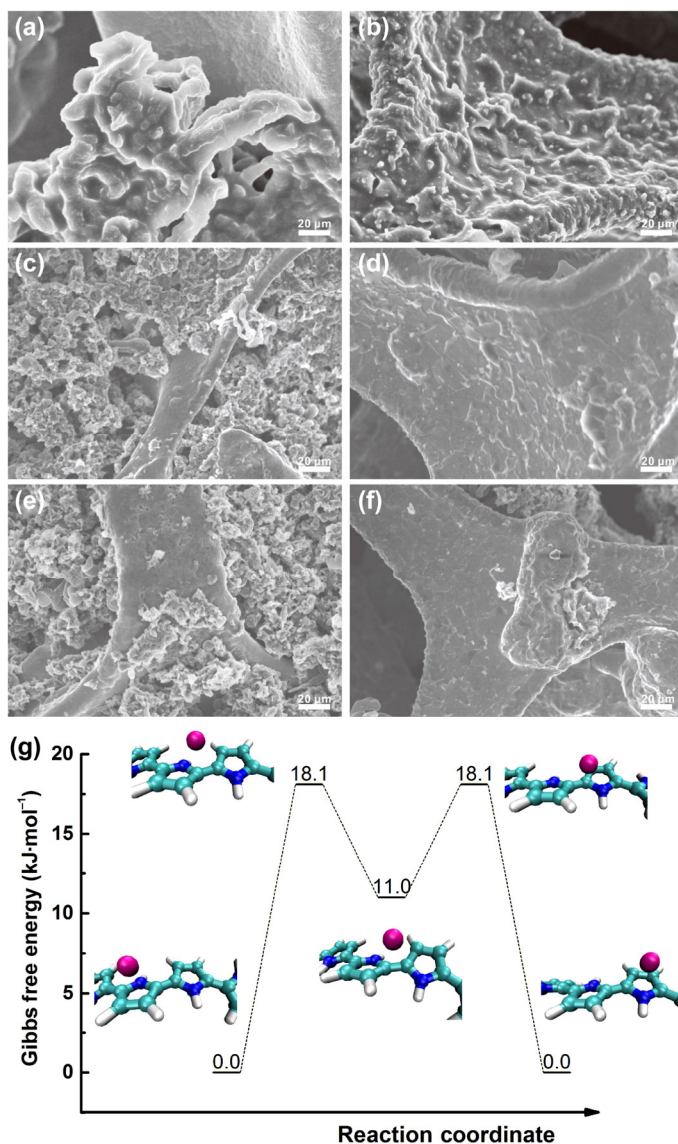


**Figure 5** The SEM images of (a) pristine Ni foam and (b) PPy@Ni foam with the Li deposition of  $5 \text{ mAh}\cdot\text{cm}^{-2}$  after 1 cycle. The SEM images of the morphologies of (c) Li plating and (e) stripping on the pristine Ni foam after 50 cycles. The SEM images of the morphologies of (d) Li plating and (f) stripping on the PPy@Ni foam after 50 cycles. (g) Migration pathway of  $\text{Li}^+$  on PPy at M06-2X-D3/def2-TZVP//M06-2X-D3/def2-SVP with SMD.

Coulombic efficiency of 99% for nearly 250 cycles. In contrast, the Coulombic efficiency of pristine Ni foam rapidly decreases after 100 cycles. When the amount of Li metal deposition increases to 5 and  $10 \text{ mAh}\cdot\text{cm}^{-2}$ , the PPy@Ni foam is still able to maintain stable lithium stripping/plating within 90 cycles and 60 cycles, respectively. Those notable improvements in the cycling performance owe to the prevention in formation of Li dendrite and stabilization in the electrolyte/electrode interface by use of PPy protective layer. What's more, the PPy protective layer can also prevent the Li metal contacting with electrolyte, thereby hindering the formation of dead Li and the loss of Li metal active material. In short, it has been proven that the PPy protective layer can effectively improve electrochemical performances of Li metal-based battery. The success of PPy protective layer has suggested that organic polymer can be chosen as protective layer for dendrite-free Li anode, providing more possibilities for the Li metal protection.

## Acknowledgements

This work is supported by the National Natural Science Foundation

of China (Nos. 2127318, 21621091 and 21875195), the National Key Research and Development Program of China (No. 2017YFB0102000), and the Fundamental Research Funds for the Central Universities (No. 20720190040).

**Electronic Supplementary Material:** Supplementary material (the electrochemical of PPy@Ni foam, the weight of PPy@Ni foam, comparison of previous work) is available in the online version of this article at <https://doi.org/10.1007/s12274-019-2481-x>.

## References

- Cheng, X. B.; Zhang, R.; Zhao, C. Z.; Zhang, Q. Toward safe lithium metal anode in rechargeable batteries: A review. *Chem. Rev.* **2017**, *117*, 10403–10473.
- Kim, H.; Jeong, G.; Kim, Y. U.; Kim, J. H.; Park, C. M.; Sohn, H. J. Metallic anodes for next generation secondary batteries. *Chem. Soc. Rev.* **2013**, *42*, 9011–9034.
- Tarascon, J. M.; Armand, M. Issues and challenges facing rechargeable lithium batteries. *Nature* **2001**, *414*, 359–367.
- Goodenough, J. B.; Park, K. S. The Li-ion rechargeable battery: A perspective. *J. Am. Chem. Soc.* **2013**, *135*, 1167–1176.
- Wang, J.; Yin, Y. B.; Liu, T.; Yang, X. Y.; Chang, Z. W.; Zhang, X. B. Hybrid electrolyte with robust garnet-ceramic electrolyte for lithium anode protection in lithium-oxygen batteries. *Nano Res.* **2018**, *11*, 3434–3441.
- Li, C. L.; Wang, J.; Chang, Z. W.; Yin, Y. B.; Yang, X. Y.; Zhang, X. B. Preparation and characterization of PAN-LATP composite solid-state electrolyte. *Sci. Sin. Chim.* **2018**, *48*, 964–971.
- Cheng, X. B.; Zhang, R.; Zhao, C. Z.; Wei, F.; Zhang, J. G.; Zhang, Q. A review of solid electrolyte interphases on lithium metal anode. *Adv. Sci.* **2016**, *3*, 1500213.
- Yang, Y.; Xiong, J.; Zeng, J.; Huang, J. X.; Zhao, J. B. VGCF 3D conducting host coating on glass fiber filters for lithium metal anodes. *Chem. Commun.* **2018**, *54*, 1178–1181.
- Peng, Y. Y.; Wen, Z. P.; Liu, C. Y.; Zeng, J.; Wang, Y. H.; Zhao, J. B. Refining interfaces between electrolyte and both electrodes with carbon nanotube paper for high-loading lithium-sulfur batteries. *ACS Appl. Mater. Interfaces* **2019**, *11*, 6986–6994.
- Ma, J. L.; Yin, Y. B.; Zhang, X. B.; Yan, J. M.; Jiang, Q. Suppressing sodium dendrites by multifunctional polyvinylidene fluoride (PVDF) interlayers with nonthrough pores and high flux/affinity of sodium ions toward long cycle life sodium oxygen-batteries. *Adv. Funct. Mater.* **2018**, *28*, 1703931.
- Cheng, X. Y.; Xian, F.; Hu, Z. L.; Wang, C.; Du, X. F.; Zhang, H. R.; Chen, S. G.; Dong, S. M.; Cui, G. L. Fluorescence probing of active lithium distribution in lithium metal anodes. *Angew. Chem., Int. Ed.* **2019**, *58*, 5936–5940.
- Gao, Y.; Yi, R.; Li, Y. C.; Song, J. X.; Chen, S. R.; Huang, Q. Q.; Mallouk, T. E.; Wang, D. H. General method of manipulating formation, composition, and morphology of solid-electrolyte interphases for stable Li-alloy anodes. *J. Am. Chem. Soc.* **2017**, *139*, 17359–17367.
- Aurbach, D.; Daroux, M. L.; Faguy, P. W.; Yeager, E. Identification of surface films formed on lithium in propylene carbonate solutions. *J. Electrochem. Soc.* **1987**, *134*, 1611–1620.
- Xu, K. Nonaqueous liquid electrolytes for lithium-based rechargeable batteries. *Chem. Rev.* **2004**, *104*, 4303–4418.
- Ma, J. L.; Meng, F. L.; Yu, Y.; Liu, D. P.; Yan, J. M.; Zhang, Y.; Zhang, X. B.; Jiang, Q. Prevention of dendrite growth and volume expansion to give high-performance aprotic bimetallic Li-Na alloy-O<sub>2</sub> batteries. *Nat. Chem.* **2019**, *11*, 64–70.
- Xu, J. J.; Liu, Q. C.; Yu, Y.; Wang, J.; Yan, J. M.; Zhang, X. B. *In situ* construction of stable tissue-directed/reinforced bifunctional separator/protection film on lithium anode for lithium-oxygen batteries. *Adv. Mater.* **2017**, *29*, 1606552.
- Liu, T.; Xu, J. J.; Liu, Q. C.; Chang, Z. W.; Yin, Y. B.; Yang, X. Y.; Zhang, X. B. Ultrathin, lightweight, and wearable Li-O<sub>2</sub> battery with high robustness and gravimetric/volumetric energy density. *Small* **2017**, *13*, 1602952.
- Yang, Y.; Xiong, J.; Lai, S. B.; Zhou, R.; Zhao, M.; Geng, H. B.; Zhang, Y. F.; Fang, Y. X.; Li, C. C.; Zhao, J. B. Vinyl ethylene carbonate as an effective SEI-forming additive in carbonate-based electrolyte for lithium-metal anodes. *ACS Appl. Mater. Interfaces* **2019**, *11*, 6118–6125.
- Aurbach, D.; Zaban, A.; Gofer, Y.; Ely, Y. E.; Weissman, I.; Chusid, O.; Abramson, O. Recent studies of the lithium-liquid electrolyte interface electrochemical, morphological and spectral studies of a few important systems. *J. Power Sources* **1995**, *54*, 76–84.
- Ishikawa, M.; Morita, M.; Asao, M.; Matsuda, Y. Charge/discharge characteristics of carbon fiber with graphite structure in organic electrolytes containing lithium trifluoromethanesulfate and lithium hexafluorophosphate. *J. Electrochem. Soc.* **1994**, *141*, 1105–1108.
- Koch, V. R.; Goldman, J. L.; Mattos, C. J.; Mulvaney, M. Specular lithium deposits from lithium hexafluoroarsenate/diethyl ether electrolytes. *J. Electrochem. Soc.* **1982**, *129*, 1–4.
- Hayashi, K.; Nemoto, Y.; Tobishima, S. I.; Yamaki, J. I. Mixed solvent electrolyte for high voltage lithium metal secondary cells. *Electrochim. Acta* **1999**, *44*, 2337–2344.
- Lu, Y. Y.; Tu, Z. Y.; Archer, L. A. Stable lithium electrodeposition in liquid and nanoporous solid electrolytes. *Nat. Mater.* **2014**, *13*, 961–969.
- Ye, H.; Zheng, Z. J.; Yao, H. R.; Liu, S. C.; Zuo, T. T.; Wu, X. W.; Yin, Y. X.; Li, N. W.; Gu, J. J.; Cao, F. F. et al. Guiding uniform Li plating/stripping through lithium-aluminum alloying medium for long-life Li metal batteries. *Angew. Chem., Int. Ed.* **2019**, *58*, 1094–1099.
- Ma, L.; Kim, M. S.; Archer, L. A. Stable artificial solid electrolyte interphases for lithium batteries. *Chem. Mater.* **2017**, *29*, 4181–4189.
- Liang, X.; Pang, Q.; Kochetkov, I. R.; Sempere, M. S.; Huang, H.; Sun, X. Q.; Nazar, L. F. A facile surface chemistry route to a stabilized lithium metal anode. *Nat. Energy* **2017**, *2*, 17119.
- Choudhury, S.; Wei, S. Y.; Ozhaves, Y.; Gunceler, D.; Zachman, M. J.; Tu, Z. Y.; Shin, J. H.; Nath, P.; Agrawal, A.; Kourkoutis, L. F. et al. Designing solid-liquid interphases for sodium batteries. *Nat. Commun.* **2017**, *8*, 898.
- Zhao, Q.; Tu, Z. Y.; Wei, S. Y.; Zhang, K. H.; Choudhury, S.; Liu, X. T.; Archer, L. A. Building organic/inorganic hybrid interphases for fast interfacial transport in rechargeable metal batteries. *Angew. Chem., Int. Ed.* **2018**, *57*, 992–996.
- Besenhard, J. O.; Wagner, M. W.; Winter, M.; Jannakoudakis, A. D.; Jannakoudakis, P. D.; Theodoridou, E. Inorganic film-forming electrolyte additives improving the cycling behaviour of metallic lithium electrodes and the self-discharge of carbon–lithium electrodes. *J. Power Sources* **1993**, *44*, 413–420.
- Osaka, T.; Momma, T.; Matsumoto, Y.; Uchida, Y. Surface characterization of electrodeposited lithium anode with enhanced cycleability obtained by CO<sub>2</sub> addition. *J. Electrochem. Soc.* **1997**, *144*, 1709–1713.
- Li, W. Y.; Yao, H. B.; Yan, K.; Zheng, G. Y.; Liang, Z.; Chiang, Y. M.; Cui, Y. The synergetic effect of lithium polysulfide and lithium nitrate to prevent lithium dendrite growth. *Nat. Commun.* **2015**, *6*, 7436.
- Markevich, E.; Salitra, G.; Aurbach, D. Fluoroethylene carbonate as an important component for the formation of an effective solid electrolyte interphase on anodes and cathodes for advanced Li-ion batteries. *ACS Energy Lett.* **2017**, *2*, 1337–1345.
- Liu, Q. C.; Xu, J. J.; Yuan, S.; Chang, Z. W.; Xu, D.; Yin, Y. B.; Li, L.; Zhong, H. X.; Jiang, Y. S.; Yan, J. M. et al. Artificial protection film on lithium metal anode toward long-cycle-life lithium-oxygen batteries. *Adv. Mater.* **2015**, *27*, 5241–5247.
- Cheng, X. B.; Yan, C.; Peng, H. J.; Huang, J. Q.; Yang, S. T.; Zhang, Q. Sulfurized solid electrolyte interphases with a rapid Li<sup>+</sup> diffusion on dendrite-free Li metal anodes. *Energy Storage Mater.* **2018**, *10*, 199–205.
- Liu, S. F.; Deng, S. J.; Xie, D.; Yao, Z. J.; Zhang, L. Y.; Wang, X. L.; Tu, J. P. *In situ* solid electrolyte interphase from spray quenching on molten Li: A new way to construct high-performance lithium-metal anodes. *Adv. Mater.* **2018**, *31*, 1806470.
- Liao, K. M.; Wu, S. C.; Mu, X. W.; Lu, Q.; Han, M.; He, P.; Shao, Z. P.; Zhou, H. S. Developing a “water-defendable” and “dendrite-free” lithium-metal anode using a simple and promising GeCl<sub>4</sub> pretreatment method. *Adv. Mater.* **2018**, *30*, 1705711.
- Yan, C.; Cheng, X. B.; Tian, Y.; Chen, X.; Zhang, X. Q.; Li, W. J.; Huang, J. Q.; Zhang, Q. Dual-layered film protected lithium metal anode to enable dendrite-free lithium deposition. *Adv. Mater.* **2018**, *30*, 1707629.
- Liu, W.; Lin, D. C.; Pei, A.; Cui, Y. Stabilizing lithium metal anodes by uniform Li-ion flux distribution in nanochannel confinement. *J. Am. Chem. Soc.* **2016**, *138*, 15443–15450.
- Liu, Y. P.; Huang, K.; Fan, Y.; Zhang, Q.; Sun, F.; Gao, T.; Yang, L. W.; Zhong, J. X. Three-dimensional network current collectors supported Si nanowires for lithium-ion battery applications. *Electrochim. Acta* **2013**, *88*, 766–771.

- [40] Schechter, A.; Aurbach, D.; Cohen, H. X-ray photoelectron spectroscopy study of surface films formed on Li electrodes freshly prepared in alkyl carbonate solutions. *Langmuir* **1999**, *15*, 3334–3342.
- [41] Grimme, S.; Antony, J.; Ehrlich, S.; Krieg, H. A consistent and accurate *ab initio* parametrization of density functional dispersion correction (DFT-D) for the 94 elements H–Pu. *J. Chem. Phys.* **2010**, *132*, 154104.
- [42] Zhao, Y.; Truhlar, D. G. The M06 suite of density functionals for main group thermochemistry, thermochemical kinetics, noncovalent interactions, excited states, and transition elements: Two new functionals and systematic testing of four M06-class functionals and 12 other functionals. *Theor. Chem. Acc.* **2008**, *120*, 215–241.
- [43] Weigend, F.; Ahlrichs, R. Balanced basis sets of split valence, triple zeta valence and quadruple zeta valence quality for H to Rn: Design and assessment of accuracy. *Phys. Chem. Chem. Phys.* **2005**, *7*, 3297–3305.
- [44] Marenich, A. V.; Cramer, C. J.; Truhlar, D. G. Universal solvation model based on solute electron density and on a continuum model of the solvent defined by the bulk dielectric constant and atomic surface tensions. *J. Phys. Chem. B* **2009**, *113*, 6378–6396.
- [45] Zhao, Y.; Schultz, N. E.; Truhlar, D. G. Design of density functionals by combining the method of constraint satisfaction with parametrization for thermochemistry, thermochemical kinetics, and noncovalent interactions. *J. Chem. Theory Comput.* **2006**, *2*, 364–382.
- [46] Hehre, W. J.; Ditchfield, R.; Pople, J. A. Self-consistent molecular orbital methods. XII. Further extensions of Gaussian-type basis sets for use in molecular orbital studies of organic molecules. *J. Chem. Phys.* **1972**, *56*, 2257–2261.
- [47] Hariharan, P. C.; Pople, J. A. The influence of polarization functions on molecular orbital hydrogenation energies. *Theor. Chim. Acta* **1973**, *28*, 213–222.
- [48] Dill, J. D.; Pople, J. A. Self-consistent molecular orbital methods. XV. Extended Gaussian-type basis sets for lithium, beryllium, and boron. *J. Chem. Phys.* **1975**, *62*, 2921–2923.
- [49] Bannwarth, C.; Ehlert, S.; Grimme, S. GFN2-xTB—An accurate and broadly parametrized self-consistent tight-binding quantum chemical method with multipole electrostatics and density-dependent dispersion contributions. *J. Chem. Theory Comput.* **2019**, *15*, 1652–1671.
- [50] Humphrey, W.; Dalke, A.; Schulten, K. VMD: Visual molecular dynamics. *J. Mol. Graphics* **1996**, *14*, 33–38.
- [51] Aurbach, D.; Pollak, E.; Elazari, R.; Salitra, G.; Kelley, C. S.; Affinito, J. On the surface chemical aspects of very high energy density, rechargeable Li–sulfur batteries. *J. Electrochem. Soc.* **2009**, *156*, A694–A702.
- [52] Mermilliod, N.; Tanguy, J.; Petiot, F. A study of chemically synthesized polypyrrole as electrode material for battery applications. *J. Electrochem. Soc.* **1986**, *133*, 1073–1079.
- [53] Zhang, X. Q.; Cheng, X. B.; Chen, X.; Yan, C.; Zhang, Q. Fluoroethylene carbonate additives to render uniform Li deposits in lithium metal batteries. *Adv. Funct. Mater.* **2017**, *27*, 1605989.
- [54] Ren, X. D.; Zhang, Y. H.; Engelhard, M. H.; Li, Q. Y.; Zhang, J. G.; Xu, W. Guided lithium metal deposition and improved lithium coulombic efficiency through synergistic effects of LiAsF<sub>6</sub> and cyclic carbonate additives. *ACS Energy Lett.* **2017**, *3*, 14–19.
- [55] Wang, Y. K.; Zhang, R. F.; Pang, Y. C.; Chen, X.; Lang, J. X.; Xu, J. J.; Xiao, C. H.; Li, H. L.; Xi, K.; Ding, S. J. Carbon@titanium nitride dual shell nanospheres as multi-functional hosts for lithium sulfur batteries. *Energy Storage Mater.* **2019**, *16*, 228–235.
- [56] Pang, Q.; Kundu, D. P.; Nazar, L. F. A graphene-like metallic cathode host for long-life and high-loading lithium–sulfur batteries. *Mater. Horiz.* **2016**, *3*, 130–136.
- [57] Luo, J.; Fang, C. C.; Wu, N. L. High polarity poly(vinylidene difluoride) thin coating for dendrite-free and high-performance lithium metal anodes. *Adv. Energy Mater.* **2018**, *8*, 1701482.
- [58] Yang, G. H.; Chen, J. D.; Xiao, P. T.; Agboola, P. O.; Shakir, I.; Xu, Y. X. Graphene anchored on Cu foam as a lithiophilic 3D current collector for a stable and dendrite-free lithium metal anode. *J. Mater. Chem. A* **2018**, *6*, 9899–9905.
- [59] Cao, R. G.; Xu, W.; Lv, D. P.; Xiao, J.; Zhang, J. G. Anodes for rechargeable lithium–sulfur batteries. *Adv. Energy Mater.* **2015**, *5*, 1402273.
- [60] Ren, F. H.; Lu, Z. Y.; Zhang, H.; Chen, X. C.; Wu, S. D.; Peng, Z.; Wang, D. Y.; Ye, J. C. Pseudocapacitance induced uniform plating/stripping of Li metal anode in vertical graphene Nanowalls. *Adv. Funct. Mater.* **2018**, *28*, 1805638.
- [61] Jin, S.; Jiang, Y.; Ji, H. X.; Yu, Y. Advanced 3D current collectors for lithium-based batteries. *Adv. Mater.* **2018**, *30*, 1802014.